



Water Resources Research

RESEARCH ARTICLE

10.1029/2018WR024652

Key Points:

- A new method was developed to quantify wetland hydrologic exchange and connectivity in low relief, depressional-rich landscapes
- The method was applied in a karst landscape and highlighted the role of connectivity in water and solute export and thus landform genesis
- The method is applicable across other depressional-rich wetlandscapes, where wetland flows and connectivity drive important functions

Supporting Information:

- Supporting Information S1

Correspondence to:

D. L. McLaughlin,
mclaugd@vt.edu

Citation:

McLaughlin, D. L., Diamond, J. S., Quintero, C., Heffernan, J., & Cohen, M. J. (2019). Wetland connectivity thresholds and flow dynamics from stage measurements. *Water Resources Research*, 55, 6018–6032. <https://doi.org/10.1029/2018WR024652>

Received 22 DEC 2018

Accepted 1 JUL 2019

Accepted article online 13 JUL 2019

Published online 24 JUL 2019

Wetland Connectivity Thresholds and Flow Dynamics From Stage Measurements

Daniel L. McLaughlin¹ , Jacob S. Diamond¹ , Carlos Quintero² , James Heffernan³ , and Matthew J. Cohen⁴

¹Department of Forest Resources and Environmental Conservation, Virginia Tech, Blacksburg, VA, USA, ²Soil and Water Sciences Department, University of Florida, Gainesville, FL, USA, ³Nicholas School of the Environment, Duke University, Durham, NC, USA, ⁴School of Forest Resources and Conservation, University of Florida, Gainesville, FL, USA

Abstract Depressional wetlands are dominant features in many low-gradient landscapes, where they provide water storage and exchange. Typical basin morphology enables water storage during drier periods, when surface flow paths are disconnected and exchange is limited to slower groundwater flow paths. Under wetter conditions, wetland stage can exceed surface connection thresholds, activating surface flow paths to downstream waters. Empirical methods are needed to quantify these dynamics and thus to assess their role in landscape hydrology and associated functions. We developed a new water budget-based approach to enumerate connectivity thresholds and flows from stage measurements. We propose that this approach, termed Connectivity and Flow from Stage (CFS), has broad applicability across wetlandscapes. We applied the CFS method in the Big Cypress National Preserve, where we hypothesized that surface connectivity episodes control water and solute flux, with consequences for exported carbonate weathering products and thus for karst landform evolution. Across five study wetlands, this analysis detected surface connectivity thresholds and assessed temporal flow dynamics. Imputed connectivity thresholds were clear from stage-dependent net flow dynamics and aligned well with LiDAR-derived thresholds. Water export occurred overwhelmingly when stage exceeded these thresholds, indicating that water and solute export from these wetlands is dominated by periods of enhanced landscape connectivity. Notably, the presented CFS method can quantify wetland connectivity thresholds from stage data, even without supporting geomorphic information. This approach is useful for understanding hydrologic controls on biogeomorphic evolution in this particular karst landscape, and more broadly for inferring wetland connectivity patterns and magnitudes in other wetland settings.

1. Introduction

1.1. Wetland Hydrologic Connectivity

Wetlands are important landscape elements, providing water storage and exchange (Bullock & Acreman, 2003), as well as many attendant biogeochemical and habitat functions (Leibowitz, 2003; Marton et al., 2015). Depressional wetlands are particularly abundant features in low relief landscapes, including many archetypal “wetlandscapes” (i.e., regional mosaics of uplands and wetlands) such as the Prairie Pothole region, U.S. west coast vernal pools, Texas playas, and Carolina bays (Lane & D’Amico, 2016). These depressional wetlands, which are often referred to as geographically isolated wetlands (Tiner, 2003), are generally small but disproportionately influence water and material budgets (Cohen et al., 2016; Holgerson & Raymond, 2018), providing distributed storage and delayed release to drainage networks (Rains et al., 2016). The primary mode of that release varies across systems, resulting from both subsurface connections via groundwater flow paths (e.g., Nebraska sandhills, north Florida cypress domes; Winter, 1986; McLaughlin & Cohen, 2013) and surface connections via fill and spill dynamics (e.g., Prairie Pothole region; Leibowitz et al., 2016). These exchange dynamics are critical for assessing aggregate wetland effects on landscape water and solute budgets but remain poorly understood due to geomorphic heterogeneity among wetlands and across landscapes. To fill this knowledge gap requires new methods that can be easily applied for detailed characterization of relative magnitudes and temporal dynamics of different flow pathways (Golden et al., 2017).

Hydrologic connectivity occurs among proximate depressional wetlands and with downstream watershed elements (i.e., streams) via subsurface and surface flows (Winter & LaBaugh, 2003). The relative importance of these flow paths varies among individual wetlands, across wetlandscapes, and over time (Park et al.,

2014), with emergent effects on watershed functions (Cohen et al., 2016; Creed et al., 2017). For example, groundwater exchange can be limited in wetlands with impermeable soils (van der Kamp & Hayashi, 2009), leading to enhanced solute retention and longer times for biogeochemical processing (Marton et al., 2015). In contrast, in wetlandscapes with more permeable soils, sustained groundwater connectivity can lead to regulation and dampening of surficial aquifer and baseflow dynamics (McLaughlin et al., 2014). Although surface connectivity in depressional wetlands is typically limited in duration and frequency (Tiner, 2003), temporary connections produce ecologically important pulses of water flow, material transport, and transient aquatic corridors (Ameli & Creed, 2017; Senar et al., 2018; Smith et al., 2018). Indeed, temporal inequality of watershed exports strongly suggests periodic but important “hot moments” of surface water and solute transport (Jawitz & Mitchell, 2011). For example, variability in periodic wetland surface connections is a primary control on chloride patterns both within wetlandscapes and in downstream receiving waters (Thorslund et al., 2018). However, the absence of prolonged surface connectivity between depressional wetlands and nearby streams has been interpreted as the absence of a meaningful role in regulating the physical, chemical, or biological integrity of downstream waters, which has led to limited U.S. Federal protections (Creed et al., 2017). Enumerating the magnitude and timing of both surface and subsurface fluxes is therefore critical for a robust understanding of depressional wetland functions, and also for a rigorous basis for evaluating their regulatory protections.

Quantifying water and material fluxes from individual wetlands in low-gradient landscapes has been a challenge due to heterogeneity among wetlands and methodological constraints. Site attributes, such as topography, soil, and bedrock permeabilities (Winter, 1999), and temporal variation in climate control the mode (surface vs. subsurface) and magnitude of hydrologic exchange (Haque et al., 2018; Thorslund et al., 2018). As a result, accurate measurements of subsurface and surface fluxes often require dense distributed well networks, site-level soil property characterization, and detailed topographic information, the combination of which is often cost or time prohibitive. Importantly, surface water flows occur when wetland stage exceeds connectivity thresholds and thus are determined by fine-scale variation in wetland morphology (Winter & LaBaugh, 2003). Methods to estimate such thresholds include water level monitoring in observed surface flow paths (e.g., swales; Haque et al., 2018; McDonough et al. 2015) and analysis of high-resolution topographic data (Jones et al., 2018; Wu et al., 2018). However, wetland bathymetry and associated connectivity thresholds are often insufficiently represented in models or monitoring (Golden et al., 2017).

The importance of wetland hydrologic exchange to landscape functions and relevant policy considerations has motivated field-based and modeling methods to quantify fluxes and watershed-scale outcomes (see Golden et al., 2017). Recent advances in distributed hydrologic modeling offer an exciting frontier for assessing the aggregate role of depressional wetlands in cumulative watershed processes (e.g., Ameli & Creed, 2017; Evenson, Golden, et al., 2018; Evenson, Jones, et al., 2018). Despite their promising trajectory, these models still require empirical observations for validation, to inform process representation and, more importantly, to develop and refine mechanistic understanding of processes and dynamics. Thus, it is notable that recent literature contains few empirical studies that discern patterns of surface and subsurface connectivity in complex wetlandscapes (but see Haque et al., 2018).

1.2. Connectivity and Flow From Stage: The CFS Approach

With increasing availability of near continuous wetland stage data, empirical methods that infer hydrologic fluxes from stage variation offer an opportunity to characterize flow dynamics at fine temporal scales and across many wetland systems. For example, subdaily (e.g., 15-min) stage variation has been used to quantify daily evapotranspiration (ET) rates (e.g., Hill & Neary, 2007; Watras et al., 2017; Diamond et al., 2018) and groundwater exchange (McLaughlin & Cohen, 2013) following the original White (1932) method. More recently, this subdaily water budget approach has been applied to estimate combined surface water and groundwater exchange (hereafter net flow) when surface connections are known to occur (Van Meter et al., 2016). In this modified White method, ET (m/day) and net flow (m/day) are calculated as (Figure 1a)

$$ET = S_y(-\Delta S + 24 g), \quad (1)$$

$$\text{Net flow} = S_y(24 g), \quad (2)$$

where ΔS is 24-hr stage (m) change (positive values indicate stage increase), S_y is specific yield (dimensionless) representing the ratio of input or output water depth relative to induced stage change, g is nighttime

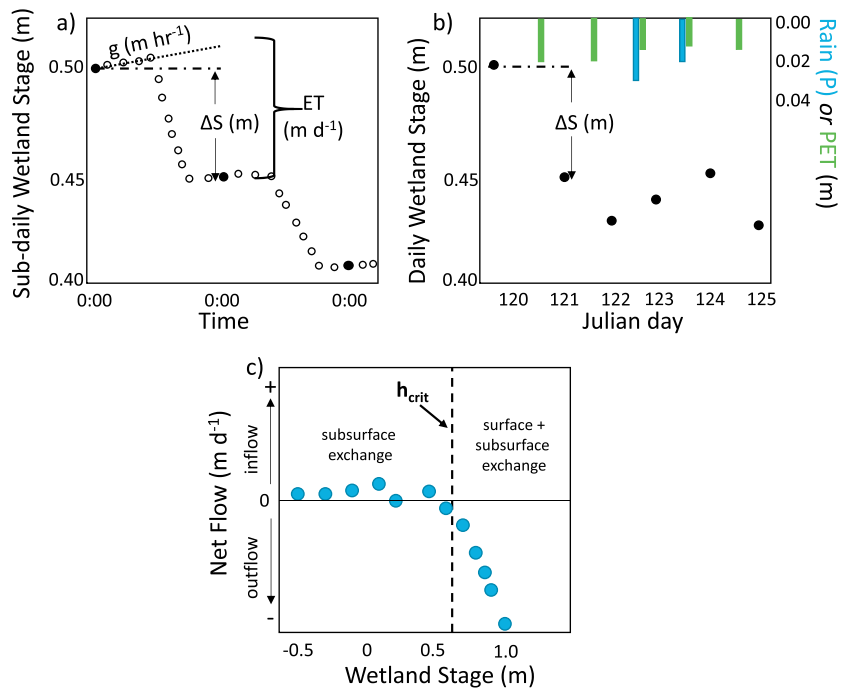


Figure 1. Different water budget approaches for estimating wetland net flows from stage: (a) the subdaily approach (equations (1) and (2)) following the original White (1932) method, which also yields estimates of evapotranspiration (ET), and (b) the daily approach (equation (3)) using daily stage, rainfall (P), and potential ET (PET) data. Open circles are 15-min stage data, and closed circles are stage at midnight. Net flow represents the combination of subsurface and surface exchange, ΔS is daily stage change (positive indicates increase), g is nighttime slope, and S_y is specific yield. (c) Predicted relationship between estimated net flows and wetland stage, where a break point pattern indicates a stage threshold (h_{crit}) for surface connections and thus when surface flows occur in addition to subsurface exchange.

slope (m/hr), and net flow is the combination of surface and subsurface flows into (+) and out of (–) of the wetland. However, this approach requires high-resolution and precision stage data to capture diel variation (McLaughlin & Cohen, 2011) and is applicable only on days without rainfall. A coarser, daily water budget approach bypasses these limitations, wherein net flow is inferred from the 24-hr stage change, adjusted for daily precipitation (P) and estimated potential ET (PET; Figure 1b):

$$\text{Net flow} = \Delta S * S_y - P + \text{PET}. \quad (3)$$

Both the daily and subdaily water budget methods yield estimates of net flows, which may be attributed exclusively to subsurface flows at low stage, but represent aggregate daily subsurface and surface flows at higher stage (Figure 1c). That is, when stage (h) is below the critical threshold for surface connectivity (h_{crit}), calculated net flows characterize subsurface exchange dynamics. Above h_{crit} , surface connectivity is activated, and net flow combines both surface and groundwater exchanges. High-resolution topographic data can be used to determine site-specific h_{crit} values and thus to distinguish surface and subsurface flows. However, we posit that quantified net flows will also yield insights about stage-dependent flow regimes (i.e., surface vs. subsurface) and thus alternative h_{crit} estimates. Specifically, we predict that relationships between quantified flows and stage will exhibit a stage-dependent discontinuity, where flows are markedly higher at stages above h_{crit} reflecting initiation of surface flow connectivity (Figure 1c). As such, we propose that stage variation can be used to (1) identify connectivity thresholds to distinguish subsurface and surface flow regimes and (2) quantify flow rates for those regimes. Here, we develop and apply this method, termed Connectivity and Flow from Stage (CFS), for broad applicability across depressional landscapes.

1.3. Study Landscape: The Big Cypress National Preserve

We apply the CFS approach in the Big Cypress National Preserve (BICY), where quantifying the various modes of, and thresholds for, hydrologic and associated solute exchange is of particular relevance to karst

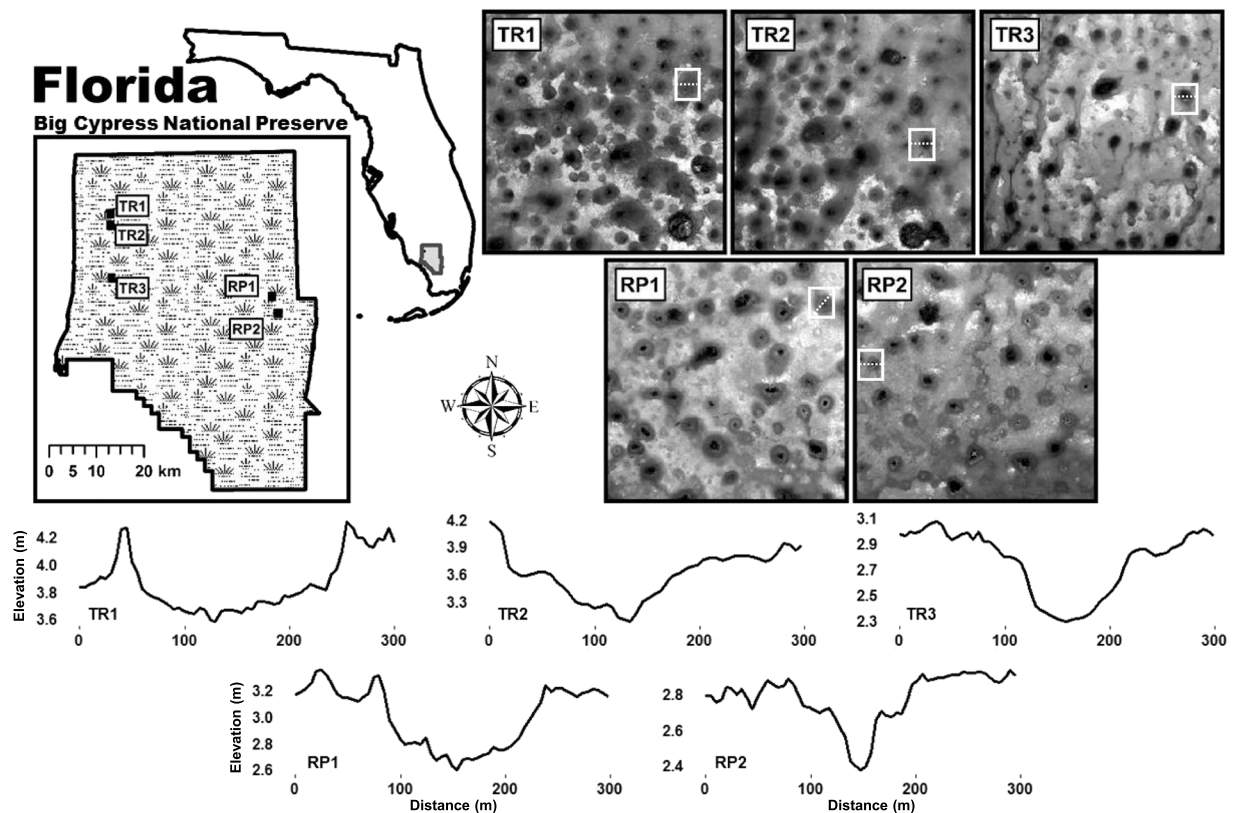


Figure 2. Big Cypress National Preserve in southwest Florida (USA) is a complex low relief mosaic of pine uplands and cypress wetlands. Numerous cypress wetland depressions are evident in LiDAR-derived digital elevation models of five landscape blocks (1.5×1.5 km each) from two main areas of Big Cypress National Preserve: Turner River (TR) and Raccoon Point (RP). Five wetland sites were selected for hydrologic investigations (boxes in each of the digital elevation models); extracted cross-sections (bottom) indicate that the basins are typically less than 1 m deep.

landform evolution. BICY is a large ($6,500 \text{ km}^2$) and extremely flat (mean slope $\sim 2 \text{ cm/km}$) patterned wetland-upland mosaic in southwest Florida, USA (Figure 2). This karst landscape is comprised of pine uplands with extremely shallow soils embedded with thousands of small wetlands. These wetlands, which are referred to as cypress domes, occur in small (mean area = 1.3 ha), regularly spaced (or patterned) depressions that cover $\sim 26\%$ of the landscape (Watts et al., 2014). Depressions are manifestations of the weathered carbonate bedrock (Pleistocene lithologies: Ft. Thompson, Tamiami formations; McPherson, 1974), with weathered minerals removed to a depth of 3 m in the wetland centers.

In BICY, wetlands depressions act as surface storage elements that appear to connect via seasonally varying surface water exchange. Despite bedrock permeability, there is limited evidence of groundwater drainage at the landscape scale. Vertical export is constrained by a thick confining unit (Hawthorn formation; McPherson, 1974), and lateral groundwater fluxes are limited by small regional head gradients (Duever et al., 1986). Consequently, the resulting flow regime is likely controlled by periods of surface water connectivity, as evidenced by rapid transitions between low- and high-discharge states in canals that drain the landscape. In other work, we have proposed that continued dissolution relies on mass export of weathered solutes during these periods of landscape discharge (Chamberlin et al., 2018; Dong et al., 2018; Watts et al., 2014). Discriminating between subsurface and surface exchanges for water and, by extension, solutes is acutely relevant to parameterizing and testing models (e.g., Dong et al., 2018) that describe millennial-scale karst pattern genesis in BICY (Chamberlin et al., 2018).

In this work, we coupled existing and refined tools for interpreting temporal variation in wetland stage with low-altitude LiDAR-derived digital elevation models to address two objectives: (1) quantify modes, magnitude, and stage thresholds of hydrologic exchange in BICY and (2) develop the proposed CFS approach for characterizing connectivity thresholds and flow dynamics using stage data alone, with broad applicability in other wetlandscapes.

2. Application

2.1. Site Descriptions

We selected a single depressional wetland from each of five landscape blocks (1.5×1.5 km) across BICY to conduct topographic and hydrologic evaluations (Figure 2). These landscape blocks are located within two main areas of BICY (Turner River [TR] and Raccoon Point [RP]) and are representative of the BICY landscape and its modest topographic and hydrologic gradients. LiDAR elevation models illustrate depressional wetland distributions (27–42% of block areas, mean = 34%) and surface flow paths in each landscape block, along with elevation cross-sections of each study wetland (Figure 2). Selected wetlands vary in bathymetry and their landscape position, including sites with and without up-gradient wetlands that contribute flow during periods of surface connectivity.

2.2. LiDAR Topographic Analysis

We used LiDAR digital elevation models (DEMs) provided by the National Center for Airborne Laser Mapping to characterize wetland bathymetry and provide topographically derived estimates of surface connectivity thresholds. LiDAR data were collected during the regional dry season (late May) to reduce impacts from standing water. DEMs spanned 2-km² block domains, capturing our sites and many other adjacent wetlands, with a reported horizontal resolution of 0.5 m, vertical resolution of 1 cm, and elevation accuracy (root mean square error [RMSE]) of 5 cm. Ground truthing of LiDAR data was not conducted in this study; however, data from two overlapping collection swaths had an RMSE of 4 to 6 cm. Preliminary visualization of the LiDAR data suggested artifacts in the bare surface DEM at the lowest elevations (i.e., dome centers) due to dense vegetation. We removed these local anomalies by resampling DEMs to 5-m pixels using a local minima filter, implemented in ArcMAP v10.5 (ESRI 2014). The resampled, 5-m DEMs also allowed for faster data processing. Processed DEM rasters were then converted to matrices using the *raster* package for R (Hijmans, 2018; R Core Team, 2016) that we then queried for inundation statistics. We estimated inundation extent for 1-cm elevation intervals (the LiDAR DEM resolution) and then constructed inundated area versus stage relationships for the local domain of each wetland. Here, the local wetland domain was defined using a bounding rectangle drawn around the wetland of interest, encompassing the entire depression feature with as little of the neighboring features as possible. These wetland-scale stage-area relationships were used to convert wetland flow rates as depth into volumetric flows (see *Hydrologic Fluxes*). We also constructed relationships at the landscape block scale (i.e., for each LiDAR block) to quantify spatially continuous inundated area extending from wetland study sites to adjacent areas.

To quantify LiDAR-derived connectivity thresholds, we used processed DEMs to delineate the wetland stage (h_{crit}) at which a wetland spills and has surface connections to adjacent areas and to the edge of the block domain. To do so, we used the Fill tool in ArcMap v10.5 to inundate the landscape up to the water elevation required to connect a wetland site to the domain edge. The difference between this elevation and ground surface at wetland wells (next section) yielded LiDAR-derived h_{crit} values relative to the wetland stage datum. To assess potential error when using the resampled 5-m DEMs, h_{crit} was extracted for one site, TR2, using both the original submeter and resampled resolution DEMs, and the derived values were within 1 cm.

2.3. Hydrologic Data Collection

To record stage at our five wetland sites (Figure 2), we installed fully screened, 3-cm wells to ~1 m below-ground in the deepest part of each wetland. We also installed groundwater wells in two surveyed upland locations adjacent to each wetland to determine daily lateral gradients between wetland and upland water levels. Each well contained a total pressure transducer (Solinst Gold Leveloggers). Barometric pressure correction was accomplished with transducers installed in vented dry wells adjacent to surface water wells (McLaughlin & Cohen, 2011). Pressure measurements were collected every 15 min from July 2014 to July 2017. Continuous precipitation depth was measured at each site with self-logging, tipping bucket gauges (HOBO RG3; Onset Corporation). Subdaily climatic data from nearby RAWS weather stations (Panther East station for TR sites; Raccoon Point station for RP sites) were used to estimate PET using the Hargreaves method (Hargreaves & Samani, 1985).

2.4. Hydrologic Fluxes

We compared the two water budget methods (subdaily and daily) to quantify combined surface and subsurface fluxes (net flow), where positive values indicate net inflow into the wetland and negative values indicate net outflow. First, we used the modified White (1932) method to extract ET (equation (1)) and net flow (equation (2)) from subdaily (15-min) variation in stage following methods in McLaughlin and Cohen (2013) and Van Meter et al., 2016; Figure 1a). This method (1) requires high-precision data to infer net flow from nighttime stage change (McLaughlin & Cohen, 2011) and (2) is not applicable on precipitation days, omitting 35% of our data record and, more importantly, periods when potentially significant flows may occur. To remedy these limitations, we applied the daily water balance approach (equation (3); Figure 1b), which obviates fine-scale data requirements and can be applied on full data records (i.e., rain and nonrain days). Note that in this approach, we do not empirically estimate ET rates but rather rely on climate-based estimates of PET and assume that actual wetland ET is equal to daily PET.

Both water budget methods require estimates of stage-dependent S_y for accurate application. For water levels below ground surface, soil S_y is applied with values dependent on water table depth and soil texture (~0.1–0.3; Healy & Cook, 2002). S_y also applies to inundated systems, where it can be assumed constant at ~1.0 for deep inundated, open water conditions (e.g., a 5-mm ET rate will induce an equivalent decrease in stage; Hill & Neary, 2007). However, under shallow inundation conditions, rapid equilibration between inundated ($S_y \sim 1.0$) and noninundated wetland locations (soil S_y) results in stage-varying S_y values (McLaughlin & Cohen, 2014), thereby requiring site-specific S_y -stage relationships. Following McLaughlin and Cohen (2014), we estimated stage-dependent S_y (i.e., ecosystem specific yield, ESY) using short-term water level responses to rainfall inputs (i.e., rain:rise [RR] ratios). Across sites, we confirmed three domains of ESY behavior: (1) constant belowground RR (mean = 0.18 ± 0.04), (2) rapidly increasing RR over a range of shallow inundation, following exponential curves (RMSE = 0.07–0.21, mean = 0.16), and (3) constant RR at high stage (mean = 0.9 ± 0.05 ; see Figure S1 in the supporting information). Estimates of ESY are critical for accurate estimation of flow magnitudes, emphasizing the value of high-resolution stage and precipitation records necessary to empirically derive this function.

Given limitations of the subdaily, modified White method, we principally used it to verify estimates from the daily water budget approach, which we then applied for complete data records (i.e., both rain and nonrain days). We further assessed the daily water budget approach by comparing estimated net flows under disconnected conditions (thus for solely groundwater exchange) to observed hydraulic gradients between wetland and upland water levels.

2.5. Surface Connectivity Thresholds from Flow Versus Stage Relationships

LiDAR-derived h_{crit} thresholds may not be available or, if so, require some independent validation. Surface connectivity thresholds may also be evident from patterns in the net flow versus stage relationship (Figure 1c). We specifically hypothesized that the activation of surface connectivity would be manifest as stage-dependent changes in net flow magnitude and that these h_{crit} values would be concordant with those extracted from LiDAR elevation analysis. Consequently, we expected that both h_{crit} and daily flows can be quantified from stage data (i.e., the CFS method). Given that ESY relationships and bathymetry may not always be available, we compared net flow versus stage relationships using three different calculations of net flow rates via the daily water budget method: (1) *uncorrected* for stage-dependent variation in S_y (i.e., assuming $S_y = 1.0$ for inundated conditions and 0.2 for noninundated conditions; Sumner, 2007); (2) *corrected* for stage-dependent S_y (via ESY extracted from RR ratios); and (3) *volumetric*, which uses wetland-scale stage-area relationships to convert corrected depth-based rates to volumes. Our goal was to evaluate whether extracted h_{crit} values were similar across these calculation methods, which would indicate that thresholds can be obtained from stage variation alone (i.e., even where ESY relationships and stage-area relationships from LiDAR terrain maps are not available). To help visualize net flow versus stage relationships, we applied standard Loess fits using the `ggplot2` package (Wickham, 2016).

Across the three different calculation methods, we assessed break points in observed net flow-stage relationships via piecewise linear regressions and rejected the null hypothesis that no break points are present using the *davies.test* function from the *segmented* package in R (Muggeo, 2008) at a significance threshold of $p = 0.05$. Where the null hypothesis could be rejected, we fitted a piecewise two-slope function using

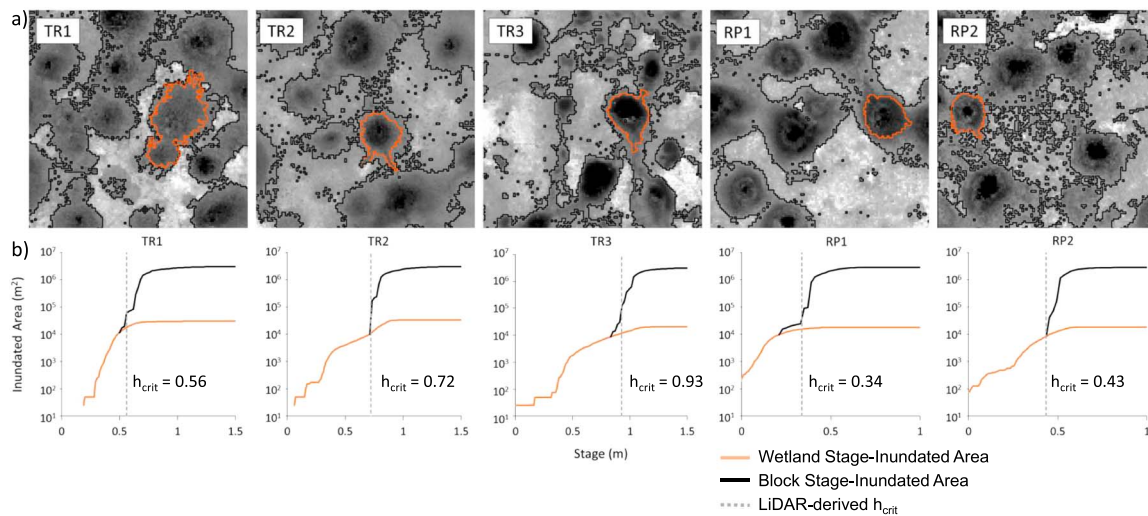


Figure 3. (a) High-resolution digital elevation model derived from low-altitude LiDAR data used to develop stage-inundated area relationships and determine stage thresholds for surface connections (h_{crit}). Orange contours denote our individual wetland sites. Black contours denote the h_{crit} elevation with an additional 10 cm of inundation and is representative of elevations at which these wetlands have activated surface connections to other wetlands and across the landscape blocks. (b) Stage-inundated area relationships for wetland site domains (orange) and the entire LiDAR blocks extending from study wetlands (black). TR = Turner River; RP = Raccoon Point.

iteratively reweighted least squares regression with the *segmented* function from the same R package. To avoid event-driven variation due to run-in on rain days, we conducted this comparison only for nonrain days. Break point estimates were compared among CFS methods and with LiDAR-derived thresholds to assess the efficacy of using stage information alone (and by extension the necessity of additional site information) to infer thresholds (h_{crit}) in wetland surface connectivity.

2.6. Site and Flow Comparisons

We assessed the magnitude and timing of flow modes (subsurface vs. surface) over the full data record for each site to formally test the hypothesis that most flow occurs when wetland stage is above h_{crit} , with implications for landscape water and solute export. To do so, we calculated cumulative flow volumes, classified into net inflow (+) and outflow (−), for each wetland as a function of stage, and observed both the frequency and cumulative magnitudes of subsurface ($h < h_{crit}$) versus combined subsurface and surface ($h > h_{crit}$) flows.

3. Results

3.1. LiDAR-Derived Connectivity Thresholds

Topographic analysis yielded critical stage thresholds (h_{crit}) that create surface connections between study wetlands (maximum extent delineated as orange lines; Figure 3a) and adjacent wetlands, resulting in a connected wetland network that extended to the block domain edge (black lines; Figure 3a). At some sites (TR3 and RP1), inundated area extended beyond delineated wetland domains before h_{crit} was reached, illustrated by the divergence between wetland- and block-scale stage-area relationships at $h < h_{crit}$ (orange vs. black lines in Figure 3b). In these cases, study wetlands reached their maximum inundation (orange lines) and then merged with adjacent wetlands (i.e., increases in block-scale inundation; black lines) but before surface connections occurred across the block domain. However, clear alignment between h_{crit} values and steep increases in block-scale stage-area relationships supports estimated stage thresholds for landscape-scale connections and highlights their role in landscape-scale inundation (Figure 3b). LiDAR-derived h_{crit} values and wetland stage time series delineated the timing and duration of surface connectivity (i.e., $h > h_{crit}$) that were remarkably similar across sites despite variation in h_{crit} (Figure 4), with significant temporal concordance (Kendall's $W = 0.79$, where values =1.0 indicate high concordance; $p = 0.002$).

3.2. Hydrologic Fluxes

Stage time series enabled quantification of hydrologic fluxes, where subdaily stage variation and the modified White method yielded both net flow rates and ET. Resulting ET:PET ratios were near unity

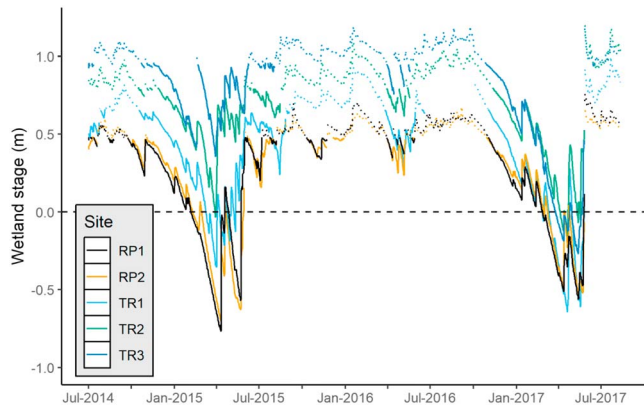


Figure 4. Stage time series for the five study wetlands. Solid lines represent times when wetland stage is below LiDAR-derived connectivity thresholds (h_{crit}), whereas dashed lines represent times when wetland stage is above h_{crit} . Dashed horizontal line denotes ground surface. TR = Turner River; RP = Raccoon Point.

(0.80 to 1.10; mean = 0.92) with significant correlations between ET and PET (Pearson's $r = +0.65-0.75$; mean = 0.70), supporting the use of the daily water balance and the assumption of $ET = PET$ for alternative estimates of net flow rates. Comparing net flow estimates from both water budget methods revealed agreement across sites ($r = +0.80-0.88$; mean $r = +0.83$). We also compared net flows estimated with the daily water budget approach when $h < h_{crit}$ (i.e., subsurface exchange only) to observed daily head gradients between wetland stage and surrounding upland groundwater levels (as an alternative indicator of groundwater exchange). Across sites, estimated net subsurface exchange from the daily water budget method was concordant with measured head gradients (Pearson's $r = +0.64-0.74$, mean $r = +0.71$). Together these comparative results support use of the daily water budget for estimating the sign and magnitude of net water exchange, expanding inference to all days (not just nonrain) and enabling use of lower resolution daily data for the CFS approach to yield both flows and connectivity thresholds.

3.3. Surface Connectivity Thresholds from Flow Versus Stage Relationships

Relationships between net flows and stage varied across the different flow calculation methods, but all produced clear stage-dependent patterns (see Figure 5 for TR2 and Figure S2 for all other sites). The simplest approach (where stage variation is uncorrected for ESY) artificially accentuates variation in net flow rates (approximately -4 to 2 cm/day; Figure 5a), particularly at low stage. However, we observed a consistent pattern across all sites, with large outflow ($-$) rates at low stage decreasing with increased stage, followed again by rapidly increasing outflow above a stage threshold (~ 0.8 m in Figure 5a). By comparison, corrected net flow rates (Figure 5b), estimated after adjusting for site-specific ESY patterns (inset), reduced both the variation and magnitude of calculated rates. The inclusion of ESY also resulted in a different flow pattern with stage, where small but consistent inflow occurred at lower stages. As with uncorrected approach, however, corrected outflows were small until stage exceeded a clear threshold (~ 0.81 m; Figure 5b). Finally, application of wetland-specific stage-area relationships (Figure 3b, orange lines) yielded volumetric flow rates (Figure 5c) and demonstrated a clearer threshold effect. Volumetric flow patterns highlighted a substantial increase in outflow magnitude above a threshold (~ 0.84 m), rendering inflow magnitudes negligible below this threshold. Net flows reported as both depth and volume rates exhibited similar patterns with increasing stage across all five sites (Loess curves in Figure 6).

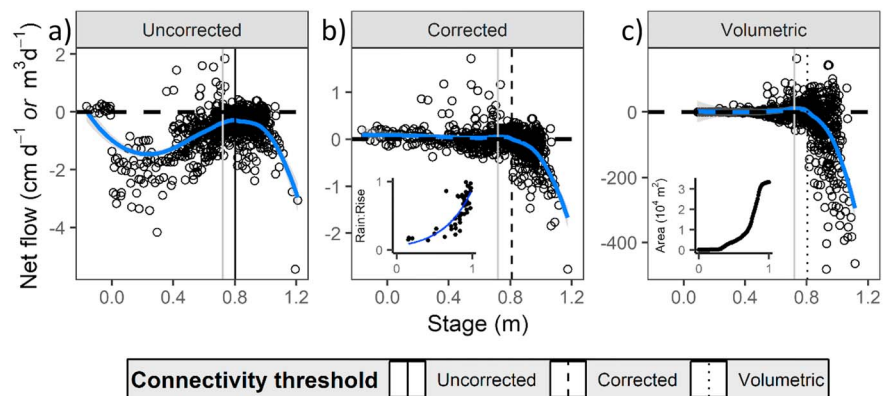


Figure 5. Comparison of Connectivity and Flow from Stage methods to estimate net flow (groundwater plus surface) for Site TR2 using the daily water budget approach: (a) uncorrected, with $S_y = 0.2$ for belowground water levels and $S_y = 1.0$ for inundation; (b) corrected for stage-dependent S_y values (ecosystem specific yield via from rain:rise estimates; inset); and (c) volumetric fluxes using stage-area relationships (inset) to convert depth-based flows. Note that volumetric fluxes are only shown for positive stage. Loess fits are shown in blue. Stage thresholds of surface connections (h_{crit}) as identified through break point analysis using flow estimates from the three different approaches and also from LiDAR (in light gray) analysis are also shown. See Figure S2 for other sites.

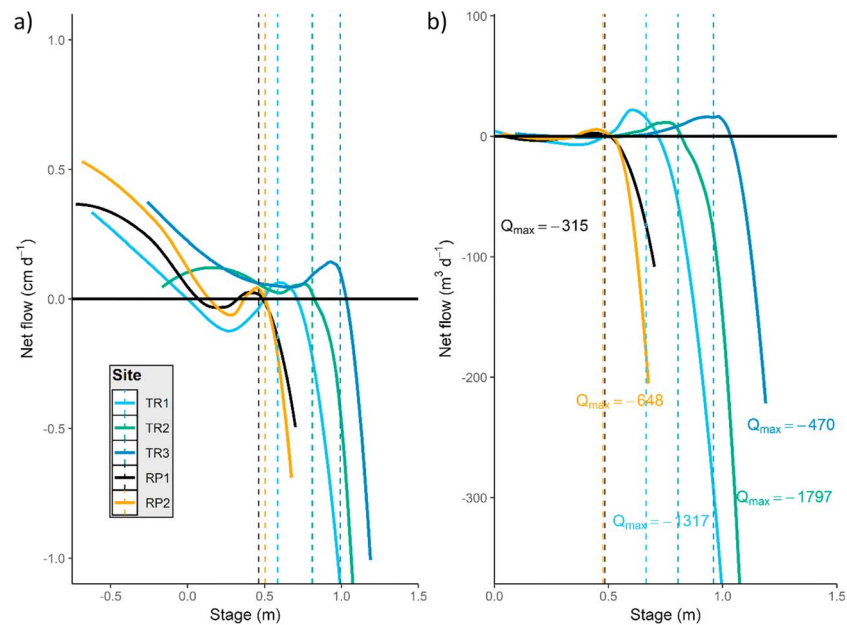


Figure 6. Loess-fitted relationships between net flow rates and stage for all five study sites for (a) corrected, depth-based and (b) volumetric fluxes. Surface connectivity thresholds (h_{crit}) are also shown for each site (dashed vertical lines). TR = Turner River; RP = Raccoon Point.

Break point analysis applied to all three CFS approaches (uncorrected, corrected, and volumetric) yielded strikingly similar estimates of h_{crit} for landscape connectivity (vertical lines in Figures 5 and 6 and Table 1). These estimates were also well aligned with thresholds derived from LiDAR analysis (Table 1), with an average difference between volumetric flow-based and LiDAR-derived thresholds of 9.8 cm.

3.4. Site and Flow Comparisons

Cumulative volumetric flows, classified as net inflow (+) and outflow (–), with increasing stage exhibited the same behavior across sites (Figure 7). Net flows below h_{crit} were small for inflows and even more so for outflows. In contrast, net inflows and outflows above h_{crit} were dramatically increased, contributing to 47–70% (mean = 59%) of cumulative inflows and 78–96% (mean = 89%) of outflows over the 3-year record. Net outflows under surface-connected conditions occurred for 13–60% (mean = 33%) of the study period (Figure 7), indicating that ~90% of the landscape discharge occurs in roughly 30% of the time. Comparisons between surface and groundwater flow paths further illustrated the extent to which hydrologic exchanges are amplified above the connectivity threshold, where combined surface and subsurface flows greatly exceeded solely subsurface exchange under disconnected conditions (Figure 8).

4. Discussion

Patterns of water storage, flux, and flow paths are the foundation of a multitude of landscape functions (Rains et al., 2016). Empirical methods that accurately quantify hydrologic exchange and connectivity are thus critically important (Spence, 2010; Phillips et al., 2011; Bracken et al., 2013), particularly in low-relief, depressional landscapes with complex mosaics of water storage and conveyance. In these wetlandscapes, the primary mode of connectivity may be surface (e.g., Prairie Pothole region, west coast vernal pools; Leibowitz & Vining, 2003; Rains et al., 2008), subsurface (e.g., Nebraska sandhills; Winter, 1986), or a time-varying combination of both (e.g., Delmarva peninsula; Evenson, Jones, et al., 2018). However, tools for quantifying these hydrologic exchange dynamics are frustratingly limited, but nonetheless crucial for understanding how

Table 1
Identified Stage Thresholds (m) for Surface Connections (h_{crit}) Derived From LiDAR and via Break Point Analysis of Flow Versus Stage Relationships Using Three Different Daily Water Budget Approaches

Site	LiDAR derived	Uncorrected	Corrected	Volumetric	C.V.
TR1	0.56	0.58	0.70	0.67	0.08
TR2	0.72	0.79	0.81	0.84	0.02
TR3	0.93	0.96	1.00	0.96	0.02
RP1	0.34	0.46	0.46	0.49	0.03
RP2	0.43	0.50	0.51	0.48	0.03

Note. TR = Turner River; RP = Raccoon Point; Coefficients of variation (C.V.) across thresholds estimates for each site are also shown.

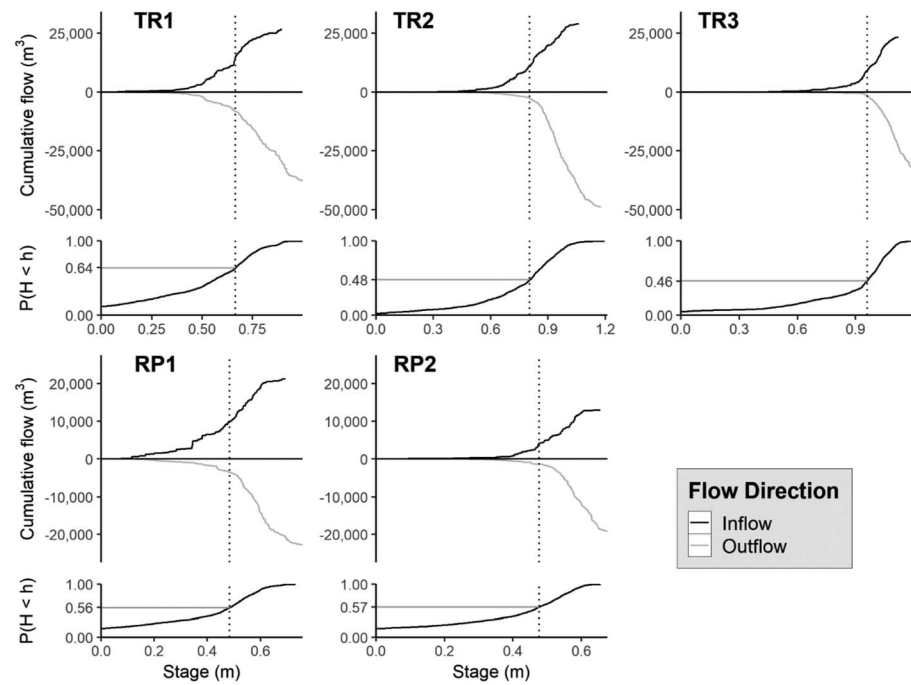


Figure 7. Cumulative volumetric flows for each site as a function of stage over the period of study, distinguished by net inflows (+, black lines) versus outflows (–, gray lines). Dotted vertical lines denote surface connection thresholds (h_{crit}) per break point analysis on volumetric flows. Cumulative frequency distributions of stage are also shown. TR = Turner River; RP = Raccoon Point.

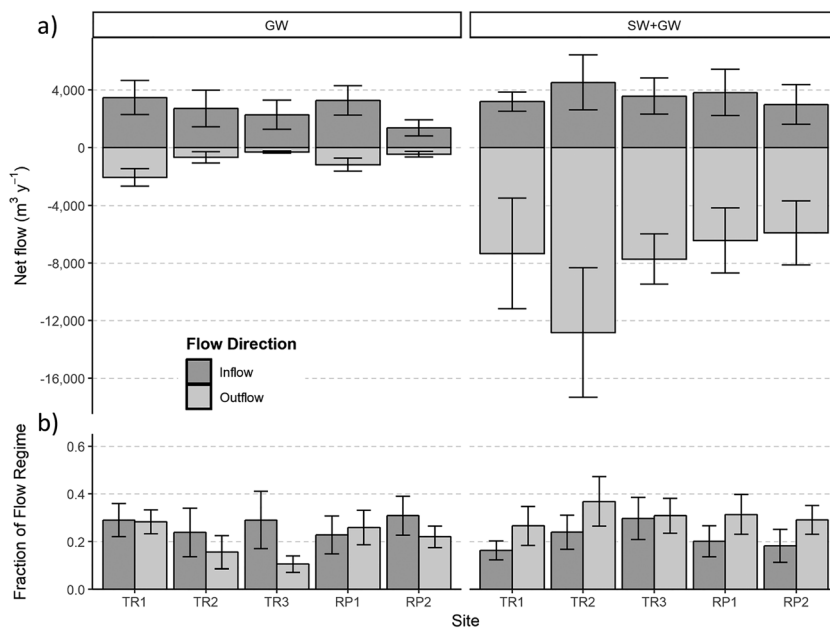


Figure 8. (a) Average annual net flows for each site over the study record (2014–2017), with standard deviations shown as error bars. Left panel (GW) presents cumulative flows under surface disconnected conditions ($h < h_{crit}$) and thus solely groundwater flows; right panel (SW+GW) presents both surface and groundwater flows when $h \geq h_{crit}$. (b) Average annual fraction of flow regime below (left panel) and above (right panel) h_{crit} . TR = Turner River; RP = Raccoon Point; GW = groundwater; SW = surface water.

wetlands impact hydrologic, biogeochemical, and biological functions (Cohen et al., 2016; Leibowitz, 2003). Our work here suggests that water level variation in depressional wetlands can reliably inform both hydrologic flows (direction and volumes) and connectivity thresholds, above which surface flow paths are activated. For the BICY landscape, the presented CFS method clearly revealed that surface flow paths, activated when water levels exceed the spill elevation, dominate total water export. While this has important landscape-specific implications for bedrock weathering and karst basin evolution, the CFS method has broader applicability. Indeed, because there is an urgent need to quantify the timing and magnitude of hydrologic exchanges to understand landscape functions, this method is likely to be informative across all manner of wetlandscapes.

4.1. Water Budgets for Wetland Connectivity Thresholds and Flows

The CFS method enables simultaneous quantification of flow rates and surface connectivity thresholds, capturing three key facets of wetland hydrologic function: the mode, magnitude, and timing of hydrologic exchange. We principally used the daily water balance approach in the CFS method because such an approach does not require high temporal resolution stage data and can be used across full data records (i.e., days with and without precipitation). This approach relies on the assumption that actual wetland ET is equal to PET, and our estimates of ET:PET from the White method suggest this is reasonable, particularly under wet conditions (water levels to ~0.5 m below the ground surface). We expect ET:PET to depart from unity under drier and deeper water table conditions, yielding errors in estimated flow at these low stages without site-specific ET information. However, in the BICY setting, and all others where flow occurs predominantly during inundated conditions, the assumptions are reasonable, particularly for the delineation of surface connectivity thresholds.

The CFS method provides estimates of flow rates and connectivity thresholds based only on stage data, obviating some challenges associated with other methods. Specifically, the method does not require a priori identification of flow path connection features (e.g., swales and artificial ditches) for high-frequency monitoring (Haque et al., 2018; McDonough et al. 2015). It also provides estimates of connectivity thresholds even where high-resolution topography is not available (Jones et al., 2018; Wu et al., 2018) and supports inferences from topographic information where stage data are limited. Indeed, connectivity thresholds obtained from analysis of LiDAR topography (Figure 3) aligned well with those from net flow versus stage relationships (Table 1), even with no prior knowledge of wetland shape, size, or connectivity features.

Both LiDAR analysis and the CFS method delineated spilling (i.e., domain-scale export) as opposed to merging (i.e., combined closed-basin storages) surface connectivity (Leibowitz et al., 2016). That is, our topographic approach identified stage thresholds for surface connections across the defined landscape block and not those that solely initiate local merging with adjacent wetlands (Figure 3b). Alignment between LiDAR-derived thresholds and those from CFS analysis implies that the latter similarly delineates stages at which landscape-scale connections and export occur. The ability to capture this scale of connectivity is important because thresholds of merging connectivity impact regional flow generation far less than thresholds of spilling connectivity (Leibowitz et al., 2016; Leibowitz & Vining, 2003). That these are clearly distinct in this extremely low relief landscape animates the capacity to discriminate among these modes of connectivity.

While there was general alignment among methods, LiDAR-derived h_{crit} values were consistently lower compared to those estimated with the CFS approach. LiDAR-derived values represent the stage that initiates continuous inundation across a delineated landscape block, but surface exchange may be minimal without further increases in stage for sustained surface flows. Further, the landscape block size was arbitrary, and a larger block may result in a higher stage threshold for block-scale connectivity. The CFS method offers a more empirical approach by identifying stage-dependent break points in net flows and thus surface exchange of magnitudes that affect individual wetland water budgets.

The modest differences between LiDAR- and CFS-derived h_{crit} values may result in potentially important differences in the imputed timing and magnitude of surface connections. For example, at TR1, where method differences in h_{crit} were greatest (Table 1), LiDAR-based estimates suggested surface connectivity occurred over 52% of the study period compared to 42% using CFS estimates. The importance of these differences is application dependent but is likely to be less important where the goal is to compare connectivity thresholds and flow path modes among regional wetland systems and across different wetlandscapes.

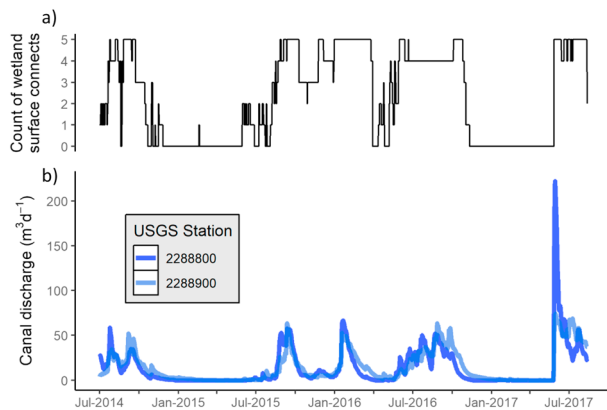


Figure 9. (a) Time series of the number of study wetlands with surface connections ($h \geq h_{crit}$) and (b) time series of discharge for two canals draining Big Cypress National Preserve. Note the coincidence of timing among surface connections and peak flows in the two canals. USGS = United States Geological Survey.

For inference of connectivity thresholds, it is notable that all three CFS calculation methods converge (i.e., uncorrected, corrected, and volumetric; Figure 5; Table 1). As such, even where S_y , ET rates, or topographic information are unavailable, stage variation can delineate surface connectivity (Figure 5a). This is relevant because while archived stage data are increasingly available, we often lack the high-resolution stage and rainfall data necessary for S_y estimates, or wetland topography necessary to estimate volumetric fluxes. We posit that inference of connectivity and flow path partitioning is still tenable with stage data alone, greatly expanding the geographic scope over which hydrologic exchange dynamics can be readily assessed. Despite this optimism for obtaining connectivity thresholds, we note significant error in flow magnitudes and even direction (Figure 5a versus 5b) using the simplest CFS approach (i.e., uncorrected for ESY), highlighting the value of stage-dependent S_y functions (ESY). Similarly, stage-area relationships from topographic data are required to convert depth-based flows to volumes (Figure 5c) and thus characterize the magnitude of wetland effects on landscape export.

Further, bathymetric data and connectivity stage thresholds together can quantify “volume to breakthrough”, a proposed unifying measure of hydrologic connectivity defined as the storage required to create downgradient discharge (Bracken & Croke, 2007). As LiDAR data become increasingly available, they will enable large-scale coupling of stage, rainfall, and topography to quantify and compare depressional hydrologic functions over complex wetlandscapes.

Several limitations of the CFS method need to be noted. First, all quantified flow rates are daily net flows, whereas gross flows are more desirable for a full landscape-integrated mass balance. That is, CFS analysis cannot parse net flows into inflow and outflow components nor can it distinguish between static (no flow) and dynamic (inflow = outflow) steady state conditions. Solute tracers offer a complimentary approach to overcome this limitation (e.g., Brooks et al., 2018), but the integrated use of these methods has not yet been fully explored. The method also cannot separately quantify surface water versus groundwater flow contributions when connectivity thresholds are exceeded; calculated net flow values are a combination of both flow paths. However, net flow versus stage relationships under subsurface flow conditions (i.e., $h < h_{crit}$) may potentially be extrapolated to estimate groundwater flows (and thus surface flows as the residual) under surface connected conditions. Finally, we again note that full implementation of CFS to yield volumetric flow rates depends on ESY and bathymetric data availability. Where these data are not available, the specificity of wetland hydrologic function is substantially reduced.

4.2. The Primacy of Threshold Connectivity for Water Export

Surface connections dominate water export in BICY at both wetland and landscape scales. In contrast to pre-conceived notions of “isolation” for depressional wetlands (Mushet et al., 2015), we observed sustained periods of surface connectivity at all sites, largely during the wet season (July–October; Figure 4). These periods of surface connectivity contributed most of the cumulative inflows ($59 \pm 9\%$) and nearly all the cumulative outflows ($89 \pm 8\%$). By complement, surface-disconnected periods during which only groundwater exchange occurs (i.e., when stage $< h_{crit}$; Figures 7 and 8) are less important in this setting. It follows that the thousands of geographically isolated wetlands that dot the BICY landscape act as a distributed but temporarily connected network that controls landscape water and solute export, as observed in other fill-and-spill wetlandscapes (e.g., Leibowitz & Vining, 2003). To further evince this hydrologic regulation function, we compared temporal patterns of wetland surface connections to landscape discharge dynamics in canals draining the landscape (Figure 9). The temporal concordance was striking and significant (Kendall’s $W = 0.910$; $p = 0.0099$): When the wetlands are collectively spilling ($h > h_{crit}$), the landscape is actively discharging water, but canal discharges effectively cease otherwise ($h < h_{crit}$).

Temporal inequality (Jawitz & Mitchell, 2011) in wetland outflows (89% of the flow in 33% of time) and canal discharges (97% of the flow during 61% of time) is clear in BICY and likely occurs in other fill-and-spill wetlandscapes, such as the Prairie Pothole region (Haque et al., 2018; Hayashi et al., 2016) and west coast vernal pools (Rains et al., 2008). Indeed, the invocation of two hydrologic states (surface connected vs.

disconnected) and associated effects on landscape discharge have been documented elsewhere (Quinton & Roulet, 1998). Additional work is needed to link wetland and landscape-scale dynamics in these settings and to draw contrast with settings where groundwater flow rates are sufficient to preclude surface spill dynamics, such as cypress domes in North Florida (McLaughlin & Cohen, 2013) and Nebraska sandhill lakes (Winter, 1986). We note that these landscapes, where connectivity is predominantly in the subsurface, do not necessarily generate less flow (Thorslund et al., 2018), which implies their support for a different portfolio of landscape functions. Many studies (e.g., McLaughlin et al., 2014; Neff & Rosenberry, 2018; Winter & LaBaugh, 2003) highlight the influences of subsurface connectivity on landscape-scale hydrology and function; we assert that the CFS method is applicable to all depressional wetland systems and will yield insights into the timing and magnitude of both surface and subsurface connectivity. Because the method works with daily water level measurements, one clear advantage is wide application across different wetlandscapes to better understand typologies and drivers of flow generating behaviors across settings.

4.3. BICY Surface Hydrology and the Export of Carbonate Weathering Solutes

Our findings have important implications for the processes thought to control landscape formation and pattern in BICY (Watts et al., 2014). Export of weathering-derived solutes is a necessary mechanism to create and expand karst depression features (Chamberlin et al., 2018), but the pathway of export has been unclear. Our results provide strong evidence that export occurs primarily via temporary surface connections. Further, despite variability in h_{crit} values across wetlands, the timing of surface connectivity was nearly identical across sites (Figures 4 and 9), implying synchronous activation of hydrochemical export, as has been observed in other patterned wetlandscapes (Quinton & Roulet, 1998). We submit that this synchrony across sites may be a unique property of patterned landscapes where biogeomorphic feedbacks dominate landform development. By extension, this synchrony is expected to be weaker in landscapes shaped by historical forcing such as glacial scour in the Prairie Pothole region, where fill-spill dynamics are highly variable among adjacent (topographically distinct) wetlands (Haque et al., 2018). Future work linking water flows with measured water chemistry will aid in assessing the role of surface connectivity in solute export, and ultimately on the emergence of self-organized, regular patterning in BICY.

5. Conclusions

The mode and magnitude of hydrologic connectivity between depressional wetlands and other watershed elements have increasingly been a focus of research and policy across many wetlandscapes (e.g., Prairie Pothole Region, Carolina and Delmarva bays, west coast vernal pools). Heterogeneity among landscape settings and even among similarly situated wetlands suggests a diverse range of wetland connectivity patterns that highlights the need for empirical tools sensitive to such site specificity. Here, we developed a new approach, termed connectivity and flow from stage (the CFS approach), to delineate connectivity thresholds and quantify subsurface and surface flows. We applied the CFS method in a low-relief, karst wetland landscape, where contemporary weathering processes are thought responsible for landform pattern. Findings demonstrated that temporary periods of surface connections overwhelmingly contributed to wetland flow generation, with important implications for weathered solute export and thus landform genesis. This system-specific relevance of surface mass flux highlights the diverse range of processes driven by hydrologic connectivity, and thus the utility of new and simple approaches to characterize that connectivity across a wide range of systems.

Acknowledgments

We gratefully acknowledge access to our BICY sites from the U.S. National Park Service (#BICY-2016-SCI-0008) and the guidance from Don Hargrove for site selection and access concerns. Field work was supported by Kenyon Watkins, Paul Decker, Brett Caudill, and Matt Kirk. Funding was provided from the National Science Foundation (DEB 1354783 and 1354750). Data are available at CUAHSI Hydroshare.

References

- Ameli, A., & Creed, I. F. (2017). Quantifying hydrologic connectivity of wetlands to surface water systems. *Hydrology & Earth System Sciences*, 21(3), 1791–1808. <https://doi.org/10.5194/hess-21-1791-2017>
- Bracken, L. J., Wainwright, J., Ali, G. A., Tetzlaff, D., Smith, M. W., Reaney, S. M., & Roy, A. G. (2013). Concepts of hydrological connectivity: research approaches, pathways and future agendas. *Earth-Science Reviews*, 119, 17–34. <https://doi.org/10.1016/j.earsci.2013.02.001>
- Bracken, L. J., & Croke, J. (2007). The concept of hydrological connectivity and its contribution to understanding runoff-dominated geomorphic systems. *Hydrological Processes*, 21(13), 1749–1763. <https://doi.org/10.1002/hyp.6313>
- Brooks, J. R., Mushet, D. M., Vanderhoof, M. K., Leibowitz, S. G., Christensen, J. R., Neff, B. P., et al. (2018). Estimating wetland connectivity to streams in the Prairie Pothole Region: An isotopic and remote sensing approach. *Water Resources Research*, 54, 955–977. <https://doi.org/10.1002/2017WR021016>
- Bullock, A., & Acreman, M. (2003). The role of wetlands in the hydrological cycle. *Hydrology and Earth Systems Sciences*, 7(3), 358–389. <https://doi.org/10.5194/hess-7-358-2003>

- Chamberlin, C., Bianchi, T., Brown, A., Cohen, M. J., Dong, X., Flint, M., et al. (2018). Mass balance implies Holocene development of a low-relief karst patterned landscape. *Chemical Geology*. <https://doi.org/10.1016/j.chemgeo.2018.05.029>
- Cohen, M. J., Creed, I., Alexander, L., Basu, N., Calhoun, A., Craft, C., et al. (2016). Do geographically isolated wetlands influence landscape functions? *Proceedings of the National Academy Sciences*, *113*(8), 1978–1986. <https://doi.org/10.1073/pnas.1512650113>
- Creed, I. F., Lane, C. R., Serran, J. N., Alexander, L. C., Basu, N. B., Calhoun, A. J. K., et al. (2017). Enhancing protection for vulnerable waters. *Nature Geosciences*, *10*(11), 809–815. <https://doi.org/10.1038/NGEO3041>
- Diamond, J., McLaughlin, D. L., Slesak, R., D'Amato, A., & Palik, B. (2018). Forested versus herbaceous wetlands: Can management mitigate ecohydrologic regime shifts from invasive emerald ash borer? *Journal of Environmental Management*, *222*, 436–446. <https://doi.org/10.1016/j.jenvman.2018.05.082>
- Dong, X., Cohen, M. J., Martin, J., McLaughlin, D. L., Murray, A. B., Ward, N., et al. (2018). Ecohydrologic processes and soil thickness feedbacks control limestone-weathering rates in a karst landscape. *Chemical Geology*. <https://doi.org/10.1016/j.chemgeo.2018.05.021>
- Duever, M. J., Carlson, J. E., Meeder, J. F., Duever, L. C., Gunderson, L. H., Riopelle, L. A., et al. (1986). *The Big Cypress National Preserve*, Research Report No. 8, (p. 447). New York, NY: National Audubon Society.
- Evenson, G. R., Golden, H. E., Lane, C. R., McLaughlin, D. L., & D'Amico, E. (2018). Depressional wetlands affect watershed hydrological, biogeochemical, and ecological functions. *Ecological Applications*, *28*(4), 953–966. <https://doi.org/10.1002/eap.1701>
- Evenson, G. R., Jones, C. N., McLaughlin, D. L., Golden, H., Lane, C. R., DeVries, B., et al. (2018). A watershed-scale model for depressional landscapes. *Journal of Hydrology X*, *1*. <https://doi.org/10.1016/j.jhydroa.2018.10.002>
- Golden, H. E., Creed, I. F., Ali, G., Basu, N. B., Neff, B., Rains, M. C., et al. (2017). Scientific tools for integrating geographically isolated wetlands into land management decisions. *Frontiers in Ecology and the Environment*, *15*(6), 319–327. <https://doi.org/10.1002/fee.1504>
- Haque, A., Ali, G., & Badiou, P. (2018). Hydrological dynamics of prairie pothole wetlands: Dominant processes and landscape controls under contrasted conditions. *Hydrological Processes*, *32*(15), 2405–2422. <https://doi.org/10.1002/hyp.13173>
- Hargreaves, G. H., & Samani, Z. A. (1985). Reference crop evapotranspiration from temperature. *Transactions of the American Society Agricultural*, *1*(2), 96–99.
- Hayashi, M., van der Kamp, G., & Rosenberry, D. O. (2016). Hydrology of prairie wetlands: Understanding the integrated surface-water and groundwater processes. *Wetlands*, *36*(S2), 237–254. <https://doi.org/10.1007/s13157-016-0797-9>
- Healy, R. W., & Cook, P. G. (2002). Using groundwater levels to estimate recharge. *Hydrogeology Journal*, *10*(1), 91–109. <https://doi.org/10.1007/s10040-001-0178-0>
- Hijmans, R. J. (2018). Raster: geographic data analysis and modeling. <https://CRAN.R-project.org/package=raster>.
- Hill, A. J., & Neary, V. S. (2007). Estimating evapotranspiration and seepage for a sinkhole wetland from diurnal surface-water cycles. *Journal of the American Water Resources Association*, *43*(6), 1373–1382.
- Holgerson, M. A., & Raymond, P. A. (2018). Large contribution to inland water CO₂ and CH₄ emissions from very small ponds. *Nature Geoscience*, *9*(3), 222–226. <https://doi.org/10.1038/NGEO2654>
- Jawitz, J., & Mitchell, J. (2011). Temporal inequality in catchment discharge and solute export. *Water Resources Research*, *47*, W00J14. <https://doi.org/10.1029/2010WR010197>
- Jones, C. N., Evenson, G. R., McLaughlin, D. L., Vanderhoof, M., Lang, M., McCarty, G., et al. (2018). Estimating restorable wetland water storage at landscape scales. *Hydrological Processes*, *32*(2), 305–313. <https://doi.org/10.1002/hyp.11405>
- Lane, C. R., & D'Amico, E. (2016). Identification of putative geographically isolated wetlands of the conterminous United States. *Journal of American Water Resources Association*, *52*(3), 705–722. <https://doi.org/10.1111/1752-1688.12421>
- Leibowitz, S. G. (2003). Isolated wetlands and their functions: An ecological perspective. *Wetlands*, *23*(3), 517–531. [https://doi.org/10.1672/0277-5212\(2003\)023\[0517:IWATFA\]2.0.CO;2](https://doi.org/10.1672/0277-5212(2003)023[0517:IWATFA]2.0.CO;2)
- Leibowitz, S. G., Mushet, D. M., & Newton, W. E. (2016). Intermittent surface water connectivity: Fill and spill vs. fill and merge dynamics. *Wetlands*, *36*(S2), 323–342. <https://doi.org/10.1007/s13157-016-0830-z>
- Leibowitz, S. G., & Vining, K. C. (2003). Temporal connectivity in a Prairie Pothole complex. *Wetlands*, *23*(1), 13–25. [https://doi.org/10.1672/0277-5212\(2003\)023\[0013:TClAPP\]2.0.CO;2](https://doi.org/10.1672/0277-5212(2003)023[0013:TClAPP]2.0.CO;2)
- Marton, J. M., Creed, I. F., Lewis, D. B., Lane, C. R., Basu, N. B., Cohen, M. J., & Craft, C. B. (2015). Geographically isolated wetlands are important biogeochemical reactors on the landscape. *Bioscience*, *65*(4), 408–418. <https://doi.org/10.1093/biosci/biv009>
- McDonough, O. T., Lang, M. W., Hosen, J. D., & Palmer, M. A. (2015). Surface hydrologic connectivity between Delmarva bay wetlands and nearby streams along a gradient of agriculture alteration. *Wetlands*, *35*, 41–53.
- McLaughlin, D. L., & Cohen, M. J. (2011). Thermal artifacts in measurements of fine-scale water level variation. *Water Resources Research*, *47*, W09601. <https://doi.org/10.1029/2010WR010288>
- McLaughlin, D. L., & Cohen, M. J. (2013). Realizing ecosystem services: Wetland hydrologic function along a gradient of ecological condition. *Ecological Applications*, *23*(7), 1619–1631. <https://doi.org/10.1890/12-1489.1>
- McLaughlin, D. L., & Cohen, M. J. (2014). Ecosystem specific yield for estimating evapotranspiration and groundwater exchange from diel surface water variation. *Hydrological Processes*, *28*(3), 1495–1506. <https://doi.org/10.1002/hyp.9672>
- McLaughlin, D. L., Kaplan, D. A., & Cohen, M. J. (2014). A significant nexus: Geographically isolated wetlands influence landscape hydrology. *Water Resources Research*, *50*, 7153–7166. <https://doi.org/10.1002/2013WR015002>
- McPherson, B. F. (1974). The big cypress swamp. In M. G. Society (Ed.), *Environments of South Florida: Present and Past*, (pp. 8–17). Miami, Florida: Miami Geological Society.
- Muggeo, V. (2008). segmented: An R package to fit regression models with broken-line relationships. *R News* *8*: 20–25.
- Mushet, D. M., Calhoun, A. J., Alexander, L. C., Cohen, M. J., Dekeyser, E. S., Fowler, L., et al. (2015). Geographically isolated wetlands: Rethinking a misnomer. *Wetlands*, *35*(3), 423–431. <https://doi.org/10.1007/s13157-015-0631-9>
- Neff, B., & Rosenberry, D. O. (2018). Groundwater connectivity of upland-embedded wetlands in the Prairie Pothole Region. *Wetlands*, *38*(1), 51–63. <https://doi.org/10.1007/s13157-017-0956-7>
- Park, J., Botter, G., Jawitz, J., & Rao, S. (2014). Stochastic modeling of hydrologic variability of geographically isolated wetlands: effects of hydro-climatic forcing and wetland bathymetry. *Advances in Water Resources*, *69*, 38–48. <https://doi.org/10.1016/j.advwatres.2014/03.007>
- Phillips, R. W., Spence, C., & Pomeroy, J. W. (2011). Connectivity and runoff dynamics in heterogeneous basins. *Hydrological Processes*, *25*, 3061–3075. <https://doi.org/10.1002/hyp.8123>
- Quinton, W. L., & Roulet, N. T. (1998). Spring and summer runoff hydrology of a subarctic patterned wetland. *Arctic and Alpine Research*, *30*(3), 285–294. <https://doi.org/10.2307/1551976>

- R Core Team. 2016. R: A language and environment for statistical computing. R Foundation for Statistical Computing, Vienna, Austria. URL: <https://www.R-project.org/>
- Rains, M. C., Dahlgren, R. A., Fogg, G. E., Harter, T., & Williamson, R. J. (2008). Geologic control of physical and chemical hydrology in California vernal pools. *Wetlands*, 28(2), 347–362. <https://doi.org/10.1672/07-132.1>
- Rains, M. C., Leibowitz, S. G., Cohen, M. J., Creed, I. F., Golden, H. E., Jawitz, J. W., et al. (2016). Geographically isolated wetlands are part of the hydrological landscape. *Hydrological Processes*, 30(1), 153–160. <https://doi.org/10.1002/hyp.10610>
- Senar, O. E., Webster, K. L., & Creed, I. F. (2018). Catchment-scale shifts in the magnitude and partitioning of carbon export in response to changing hydrologic connectivity in a northern hardwood forest. *Journal of Geophysical Research: Biogeosciences*, 123, 2337–2352. <https://doi.org/10.1029/2018JG004468>
- Smith, L. L., Subalusky, A. L., Atkinson, C. L., Earl, J. E., Mushet, D. M., Scott, D. E., et al. (2018). Biological connectivity of seasonally ponded wetlands across spatial and temporal scales. *Journal of the American Water Resources Association: doi*, 55(2), 334–353. <https://doi.org/10.1111/1752-1688.12682>
- Spence, C. (2010). A paradigm shift in hydrology: Storage thresholds across scales influence catchment runoff generation. *Geography Compass*, 4(7), 819–833. <https://doi.org/10.1111/j.1749-8198.2010.00341.x>
- Sumner, D. M. (2007). Effects of capillarity and microtopography on wetland specific yield. *Wetlands*, 27(3), 693–701. [https://doi.org/10.1672/0277-5212\(2007\)27\[693:EOCAMO\]2.0.CO;2](https://doi.org/10.1672/0277-5212(2007)27[693:EOCAMO]2.0.CO;2)
- Thorslund, J., Cohen, M. J., Jawitz, J. W., Destouni, G., Creed, I. F., Rains, M. C., et al. (2018). Solute evidence for hydrological connectivity of geographically isolated wetlands. *Land Degradation and Development*, 29(11), 4061–4070. <https://doi.org/10.1002/ldr.3175>
- Tiner, R. W. (2003). Geographically isolated wetlands of the United States. *Wetlands*, 23(3), 494–516. [https://doi.org/10.1672/0277-5212\(2003\)023\[0494:GIWOTU\]2.0.CO;2](https://doi.org/10.1672/0277-5212(2003)023[0494:GIWOTU]2.0.CO;2)
- van der Kamp, G., & Hayashi, M. (2009). Groundwater-wetland ecosystem interaction in the semiarid glaciated plains of North America. *Hydrogeology Journal*, 17, 203–217. <https://doi.org/10.1016/j.hydroa.2018.10.002>
- Van Meter, K. J., Steiff, M., McLaughlin, D. L., & Basu, N. B. (2016). The socioecohydrology of rainwater harvesting tanks in India: Understanding water storage and release dynamics across spatial scales. *Hydrology and Earth System Sciences*, 20(7), 2629–2647. <https://doi.org/10.5194/hess-20-2629-2016>
- Watras, C. J., Morrison, K. A., Rubsam, J. L., & Buffam, I. (2017). Estimates of evapotranspiration from contrasting Wisconsin peatlands based on diel water table oscillations. *Ecohydrology*, 10(4), e1834. <https://doi.org/10.1002/eco.1834>
- Watts, A. C., Watts, D. L., Cohen, M. J., Heffernan, J. B., McLaughlin, D. L., Martin, J. B., et al. (2014). Evidence of biogeomorphic patterning in a low-relief karst landscape. *Earth Surface Processes and Landforms*, 39(15), 2027–2037. <https://doi.org/10.1002/esp.3597>
- White, W.N. 1932. A method of estimating ground-water supplies based on discharge by plants and evaporation from soil. Results of investigation in Escalante Valley, Utah. US Geological Survey Water Supply Paper:1-105.
- Wickham, H. (2016). *ggplot2: Elegant graphics for data analysis*. New York: Springer-Verlag. <https://doi.org/10.1007/978-3-319-24277-4>
- Winter, T. C. (1986). Effect of ground-water recharge on configuration of the water table beneath sand dunes and on seepage in lakes in the sandhills of Nebraska, U.S.A. *Journal of Hydrology*, 86(3-4), 221–237. [https://doi.org/10.1016/0022-1694\(86\)90166-6](https://doi.org/10.1016/0022-1694(86)90166-6)
- Winter, T. C. (1999). Relation of streams, lakes, and wetlands to groundwater flow systems. *Hydrogeology Journal*, 7(1), 28–45. <https://doi.org/10.1007/s100400050178>
- Winter, T. C., & LaBaugh, J. W. (2003). Hydrologic considerations in defining isolated wetlands. *Wetlands*, 22, 532–540. <https://doi.org/10.1672/0277-5212>
- Wu, Q., Lane, C. R., Wang, L., Vanderhoof, M. K., Christensen, J. R., & Liu, H. (2018). Efficient delineation of nested depression hierarchy in digital elevation models for hydrological analysis using level-set method. *Journal of the American Water Resources Association: doi*, 55(2), 354–368. <https://doi.org/10.1111/1752-1688.12689>